

Ground-state path integral Monte Carlo simulations of positive ions in ${}^4\text{He}$ clusters: bubbles or snowballs?

Stefano Paolini,^{1,2,*} Francesco Ancilotto,^{1,2,†} and Flavio Toigo^{1,2,‡}

¹ – Dipartimento di Fisica "G. Galilei", Università di Padova, via Marzolo 8, I-35131 Padova, Italy

² CNR-INFM-DEMOCRITOS National Simulation Center, Trieste, Italy

(Dated: November 1, 2018)

The local order around alkali (Li^+ and Na^+) and alkaline-earth (Be^+ , Mg^+ and Ca^+) ions in ${}^4\text{He}$ clusters has been studied using ground-state path integral Monte Carlo calculations. We apply a criterion based on multipole dynamical correlations to discriminate between solid-like versus liquid-like behavior of the ${}^4\text{He}$ shells coating the ions. As it was earlier suggested by experimental measurements in bulk ${}^4\text{He}$, our findings indicate that Be^+ produces a solid-like ("snowball") structure, similarly to alkali ions and in contrast to the more liquid-like ${}^4\text{He}$ structure embedding heavier alkaline-earth ions.

PACS numbers: 36.40.-c, 36.40.Mr, 67.40.Yv, 67.70.Jg, 02.70.Ss

I. INTRODUCTION

In past decades, the implantation of ions in liquid helium has often been used to probe the bulk properties of the superfluid state.¹ The attention has also focused on the details of the structure of the helium solvent around the ions.^{2,3,4} As a consequence of electrostriction, a strong increase in the helium density with respect to its bulk value is expected in the surroundings of the impurity site.^{2,3} Within a crude picture, ions in liquid helium can be divided in two categories, on the basis of the different local structure they create in the solvent. Strongly attractive ions tend to form a *solid-like* structure, the so-called *snowball*, characterized by a very inhomogeneous helium density in the surroundings of the impurity. Alkali ions are believed to belong to this category. In contrast, singly charged alkaline-earth cations, due to their larger radii and weaker interaction with the He atoms, are expected to produce a cavity surrounded by compressed, less structured, and most likely *not solidified*, helium (*bubble* in the following).³

Several investigations of the ion-helium structure have been based on measurements of ions mobilities in bulk helium.^{5,6} In particular, the experimental results of Ref. 6 have shown that the temperature dependence of the mobility of Be^+ is much more similar to that of alkali ions (K^+ , Rb^+ and Cs^+)⁵ and He^+ ,⁶ than to that of the other alkaline-earth ones (Mg^+ , Ca^+ , Ba^+ , Sr^+).⁶ It was thus suggested that Be^+ forms a snowball, similarly to He^+ and alkali ions, and at variance with heavier alkaline-earth ions, where "bubble" states are believed to develop instead.⁶ The recent discovery that positive ions can be captured in helium nanodroplets⁷ promises an extension to charged particles of experimental techniques which proved extraordinarily fruitful for neutral species.^{8,9,10}

Quantum many-body simulation methods allow for a microscopic description of such systems,^{11,12} as well as for the investigation of solid-like behavior in quantum clusters.¹³ Using quantum Monte Carlo (QMC) simulations, within the shadow wave function approach, different pos-

itive ions have been studied both in bulk ${}^4\text{He}$,^{11,14} and ${}^4\text{He}$ clusters,¹⁴ with the aim of computing the effective masses of charged impurities moving in liquid ${}^4\text{He}$ and of establishing, at the same time, the surrounding local structure of the solvent (for a calculation of the effective masses within the hydrodynamical model see Ref. 15).

The distinction between solid- and liquid-like behavior of ${}^4\text{He}$ around atomic/molecular impurities is a subtle issue which requires a careful examination of the dynamical evolution of the system. Within reptation quantum Monte Carlo (RQMC),^{16,17} the use of suitable (imaginary) time-correlation functions has been exploited to propose a dynamical criterion for discriminating between freezing versus quantum melting in small para-hydrogen clusters.¹³ In the present paper, we resort to the same criterion to investigate the structural order in ${}^4\text{He}$ clusters doped with alkali and alkaline-earth positive ions, simulated by a more standard ground-state path integral (PIGS) Monte Carlo algorithm.¹⁸ We take Li^+ and Na^+ as representatives of alkali metals, while among the alkaline-earths, we consider Be^+ , Mg^+ and Ca^+ . Lithium and sodium -doped ${}^4\text{He}$ clusters have been chosen because the strong interaction of these ions with the ${}^4\text{He}$ solvent makes them prototypes of snowball structures, whose expected solid-like signature can provide a useful benchmark in the study of the other ions, where a clear-cut distinction between bubbles and snowballs might not be easy to be resolved. As a paradigmatic case of liquid helium-impurity structures, we also simulated a small ${}^4\text{He}$ cluster seeded with a carbon monoxide molecule. We considered ion impurities in clusters rather than in bulk helium in order to avoid the possibility of finding fictitious structures imposed by the symmetry of the periodically repeated simulation box. Moreover, the local ${}^4\text{He}$ structure around the ion in large enough clusters should be very similar to that developed in bulk ${}^4\text{He}$.¹⁴

We show that the criterion proposed in Ref. 13 is applicable also to larger systems than those investigated in that paper, and that it is able to discriminate between a crystalline or a liquid behavior of the impurity-He structure. In qualitative agreement with experimental data,⁶

our simulations show in particular that the ^4He structure around Be^+ is much more similar to that found around alkali ions, where a snowball structure is found, than to the one around heavier alkaline-earth ions, where ^4He exhibits a more liquid-like behavior.

Our paper is organized as follows. In Sec. II we briefly review our theoretical framework. Section III A contains our results for very small ^4He clusters (seeded with Li^+ and CO), that have been considered for testing our computational strategy. In Sec. III B we present simulations for several ions solvated in larger ^4He clusters, and we discuss the implications of these results on the main issue we are addressing in this paper (i.e. the local structure of the ^4He solvent around Be^+ in comparison with the findings for alkali ions and other alkaline-earth ones). Finally, Section IV contains our conclusions.

II. THEORY

Our clusters are described by a realistic Hamiltonian, \hat{H} , in which the N ^4He atoms and the ionic impurity are treated as point particles interacting via pair potentials. When the CO molecule is used as dopant, we neglect its internal degrees of freedom and we treat it as a rigid linear rotor with only translational and rotational degrees of freedom. The interactions are derived from accurate quantum chemistry calculations, either by an interpolation of tabulated values, as for $\text{Li}^+\text{-He}$ and $\text{Ca}^+\text{-He}$,^{19,20} or by parametrized analytical expression, as for He-He ,²¹ He-CO ,²² and for the remaining He-ions pairs.^{23,24} The size of the ion-doped clusters varies up to a maximum of 70 ^4He atoms, whereas, in the case of CO , we considered a smaller cluster, with only fifteen particles (CO@He_{15}), approximatively corresponding to one complete solvation shell.²⁵

We simulate the system using the ground-state path integral Monte Carlo scheme,¹⁸ where the imaginary-time evolution operator, $e^{-\beta\hat{H}}$, is exploited to improve systematically a suitable trial function Ψ_T , by projecting it out onto the state $|\Psi_\beta\rangle = e^{-\beta\hat{H}}|\Psi_T\rangle$. The latter converges to the exact ground state, Ψ_0 , for $\beta \rightarrow \infty$. By Trotter slicing the imaginary-time evolution into m time steps of length $\epsilon = \beta/m$, and by choosing an appropriate definite positive short-time approximation for the imaginary-time propagator, $G(\mathbf{R}', \mathbf{R}; \epsilon) \approx \langle \mathbf{R}' | e^{-\epsilon\hat{H}} | \mathbf{R} \rangle$ between the configurations \mathbf{R} (a vector which describes the coordinates of all ^4He atoms in the cluster, in addition to those of the impurity) and \mathbf{R}' , expectation values of quantum operators, \hat{O} , on the state $|\Psi_\beta\rangle$, can be expressed in a path-integral form:

$$\langle \hat{O} \rangle_\beta = \frac{\langle \Psi_\beta | \hat{O} | \Psi_\beta \rangle}{\langle \Psi_\beta | \Psi_\beta \rangle} \approx \int dX O(\mathbf{R}_m) P(X), \quad (1)$$

where $P(X) = \Psi_T(\mathbf{R}_0) \prod_{i=1}^{2m} G(\mathbf{R}_i, \mathbf{R}_{i-1}; \epsilon) \Psi_T(\mathbf{R}_{2m})$, $X = \{\mathbf{R}_0, \dots, \mathbf{R}_{2m}\}$ is a path of configurations of the

system, and \hat{O} is diagonal in the coordinate representation. By sampling the probability $P(X)$ via a generalized Metropolis algorithm, and accumulating the values assumed by the operator \hat{O} over the sampled paths, the desired expectation value can be accessed within a known statistical error and without any mixed estimate nor population-control bias.

For the relatively small CO@He_{15} , it is sufficient to use the primitive approximation²⁶ for the imaginary-time propagator G , and then to sample the probability $P(X)$ by the RQMC algorithm.^{16,17} In the case of ionic impurities, we resorted to the pair approximation for G ,²⁶ employing the bisection-multilevel sampling procedure.²⁶ The dependence of $\langle \hat{O} \rangle_\beta$ on β and ϵ needs to be checked, in order to extrapolate the result to the exact value. Our projection times β varied between 0.1K^{-1} and 0.7K^{-1} , while we used time steps ϵ ranging between 0.0025K^{-1} and 0.0125K^{-1} for clusters seeded with ions, and equal to 0.001K^{-1} for CO@He_{15} . These values of β and ϵ have been empirically found to ensure the stability of our results.

We used a Jastrow-type trial wave function:

$$\Psi_T = \exp \left[- \sum_{i=1}^N u_1(r_i) - \sum_{i<j}^N u_2(r_{ij}) \right], \quad (2)$$

where r_i and r_{ij} indicate, respectively, the distances between the i -th ^4He atom and the ion, and that between the i -th and the j -th ^4He atoms. The radial functions u_1 and u_2 have been optimized independently for each one of the simulated systems, by minimizing the cluster variational energy with respect to a small number (10-12) of adjustable parameters. For CO@He_{15} , the one-body term u_1 also depends on the angle between the molecular axis and the vector position of the ^4He atom with respect to the molecule center of mass (details can be found in Ref. 25).

Within the path integral scheme, \hat{O} can be either a static operator (such as the Hamiltonian itself) or a time-dependent one, such as those needed to calculate imaginary-time correlation functions, $\hat{A} \exp(-\tau\hat{H}) \hat{B}$. Their evaluation requires an extended time range, $2\beta + \tau$, but it is nevertheless straightforward: $c_{AB}(\tau) = \langle \Psi_\beta | \hat{A}(\tau_0) \hat{B}(\tau_0 + \tau) | \Psi_\beta \rangle$ is estimated as $\langle \frac{1}{n_i} \sum_i A(\mathbf{R}_i) B(\mathbf{R}_{i+k}) \rangle$, where $k = \tau/\epsilon$, $\langle \cdot \rangle$ indicates a statistical average over the sampled paths, and the n_i values of i span the range $\beta/\epsilon < i < 2m - 2\beta/\epsilon - k$. The results that will be shown in the following Sections have been obtained by varying τ within 1K^{-1} . Notice that time-translation invariance implies that these correlations are independent of τ_0 .

As it was proposed in Ref. 13, imaginary-time correlations can be exploited to unveil either a solid- or a liquid-like behavior in quantum clusters, by monitoring the persistence of geometrical signatures of a solid-like structure. The criterion of Ref. 13 is based on the definition of the rotationally invariant time-correlation functions

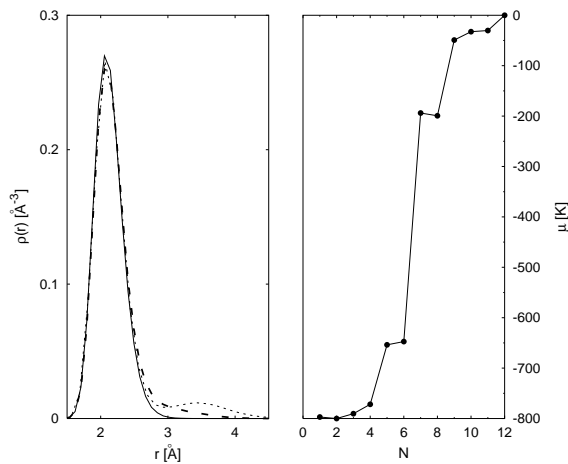


FIG. 1: Left panel: Radial density distribution of ${}^4\text{He}$ atoms around the Li^+ ion in $\text{Li}^+@{}^4\text{He}_N$ for $N = 8$ (solid line), $N = 9$ (long dashed line), and $N = 10$ (short dashed line). Right panel: ${}^4\text{He}$ chemical potential $\mu_N = E_N - E_{N-1}$ as a function of the cluster size, N , in $\text{Li}^+@{}^4\text{He}_N$, whose total energy is E_N .

$$c_L(\tau) = \frac{\sum_M \langle Q_{LM}^*(\tau_0) \overline{Q}_{LM}(\tau_0 + \tau) \rangle}{\sum_M \langle Q_{LM}^*(\tau_0) Q_{LM}(\tau_0) \rangle}, \quad (3)$$

of the multipole moments,

$$Q_{LM} = \sqrt{4\pi/(2L+1)} \int d\mathbf{r} \rho(\mathbf{r}) r^L Y_{LM}^*(\theta, \phi), \quad (4)$$

of the cluster mass distribution $\rho(\mathbf{r})$, around its center of mass. In Eq. 3, $Q_{LM}(\tau_0)$ is the multipole moment of the system at (imaginary) time τ_0 and $\overline{Q}_{LM}(\tau_0 + \tau)$ indicates the multipole calculated after the configuration at time $\tau_0 + \tau$ has been rotated back in order to minimize the particles diffusion between the two time instants.

For a rigid system $c_L(\tau)$ is independent of time, whereas it decays to zero at large τ if the system undergoes random fluctuations. A large value of $c_L(\tau)$ at large times is thus a distinctive mark of the persistence of the shape (“rigidity”) of the system. This criterion has been originally applied to small clusters of parahydrogen molecules (both pure and doped with a CO molecule), for cluster sizes around twelve molecules, at which a first solvation shell is completed.¹³ As a preliminary step in the study of the correlation functions $c_L(\tau)$, we evaluate the static multipole correlation function, $q_L = \sum_M \langle Q_{LM}^* Q_{LM} \rangle$, which provides a rotationally invariant characterization of a rigid body.¹³ This quantity is not suitable for discriminating the cases where a given multipole vanishes on average but q_L is different from zero because of fluctuations, from those where a non-vanishing q_L value is due to the average shape of the system. However, non-vanishing q_L values allow to select a set of L 's among which to search for slow-decaying time-correlations $c_L(\tau)$.

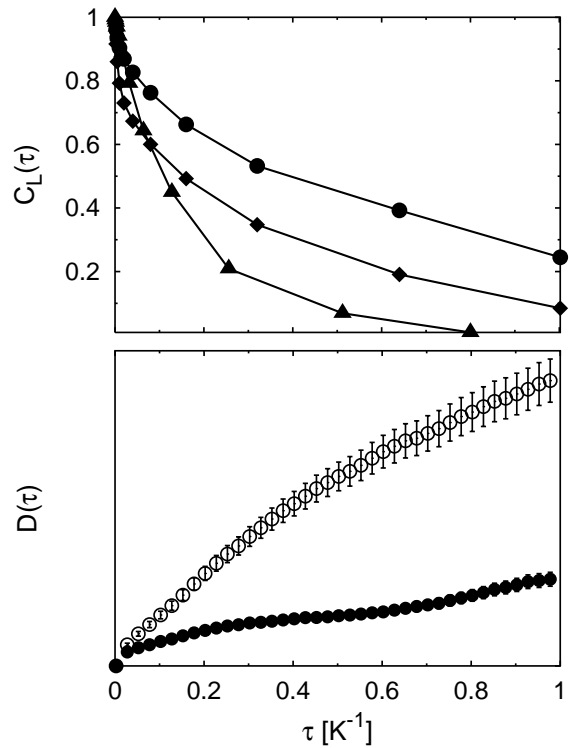


FIG. 2: Upper panel: Multipole time-correlation functions $c_L(\tau)$ of $\text{Li}^+@{}^4\text{He}_8$ ($L = 4$: diamonds, $L = 5$: filled circles) and $\text{CO}@{}^4\text{He}_{15}$ ($L = 5$: triangles). Lower panel: Diffusion coefficient of the ${}^4\text{He}$ atoms in $\text{Li}^+@{}^4\text{He}_8$, as calculated from the original configurations (empty circles) and from configurations rotated back as described in the text (filled circles).

III. RESULTS AND DISCUSSION

A. Testing the approach on small clusters

As a test case, we first discuss the results for a Li^+ ion in small ${}^4\text{He}$ clusters ($\text{Li}^+@{}^4\text{He}_N$). The left panel of Fig. 1 displays the radial distribution functions of ${}^4\text{He}$ atoms around the impurity ion, for cluster sizes in the range $N = 8 - 10$. For $N \geq 9$ the magnitude of the maximum of these functions stays nearly constant while the tail of the distribution extends to larger distances from the dopant. Correspondingly, the chemical potential rises steeply from $N = 8$ to $N = 9$. These findings indicate that for $N = 8$ a first solvation shell has been completed. We notice that an even more marked jump in the chemical potential occurs at $N = 6$, thus suggesting a great stability of $\text{Li}^+@{}^4\text{He}_6$. In particular some of the multipole imaginary-time correlation functions of $\text{Li}^+@{}^4\text{He}_6$ show an extremely slow decay in imaginary time, which is indicative of the rigidity of the system (see below). However, since we aim at revealing the existence of solid-like signatures within the first shell of larger clusters, we will not discuss any longer the case of $\text{Li}^+@{}^4\text{He}_6$, focusing instead on the solvent structure in a cluster of eight ${}^4\text{He}$ atoms, i.e. one representing a fully developed first

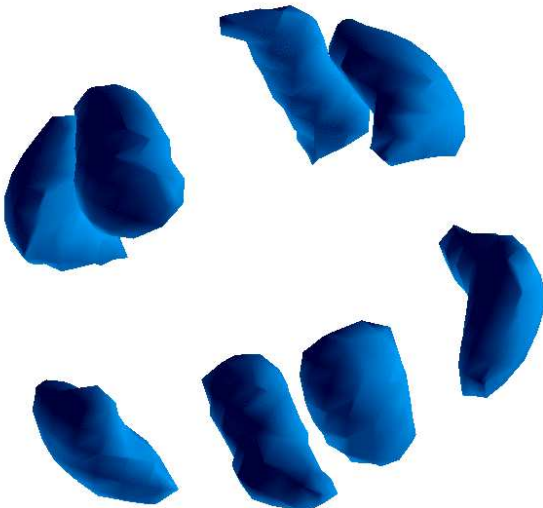


FIG. 3: He density distribution for $\text{Li}^+\text{@He}_8$. The displayed isosurface contains about 50% of the total number of He atoms. The Li^+ ion (not shown) is located at the center of the cluster.

solvation shell.

The upper panel of Fig. 2 shows the multipole time-correlation functions of $\text{Li}^+\text{@He}_8$ for $L = 4, 5$ and, for comparison, of CO@He_{15} for $L = 5$. All the multipoles correlations of CO@He_{15} decay rapidly, indicating a liquid-like behavior of the first He shell around the molecule, and we arbitrarily chose to show the $L = 5$ curve as representative of the general behavior of the $c_L(\tau)$ correlations for any L . On the other hand, in $\text{Li}^+\text{@He}_8$, all the multipole time-correlations with $L < 4$ decay rapidly, whereas for $L = 4$ and, more evidently, for $L = 5$, after a short transient in which a very steep drop occurs, the correlations decays much more slowly, indicating the long persistence of an average geometrical shape of the cluster. In the lower panel of Fig. 2 we compare the diffusion coefficient $D(\tau) = \langle \frac{1}{N} \sum_{i=1}^N [\mathbf{r}_i(\tau + \beta) - \mathbf{r}_i(\beta)]^2 \rangle$ of the ^4He atoms, as calculated from the original configurations of each quantum path generated during the simulation, with that obtained after rotating backward the configurations at time τ in order to minimize the particles diffusion with respect to the configuration at time β . The high degree of rigidity of the cluster structure near the impurity is confirmed by the considerable effectiveness of the diffusion minimization procedure.

In order to visualize the intrinsic shape of the ^4He cluster, we have calculated the helium density distribution $\bar{\rho}(\mathbf{r}) = \langle \sum_{i=1}^N \delta(\mathbf{r} - \mathbf{r}_i) \rangle$ around the ion, by applying the mentioned backward-rotation procedure. The contribution to $\bar{\rho}(\mathbf{r})$ from each quantum path sampled by the PIGS simulation is then further rotated to minimize the diffusion of the particles centroids of different paths. Fig 3 shows the density distribution for $\text{Li}^+\text{@He}_8$. The solvent accumulates in eight regions roughly arranged in

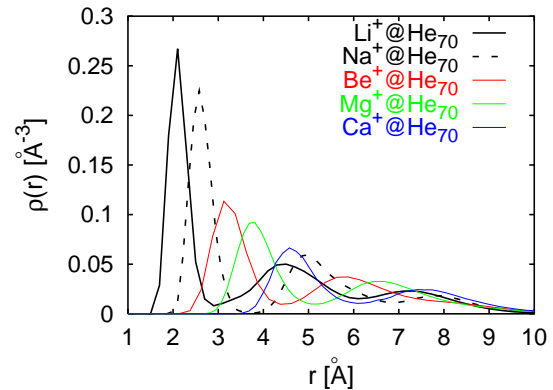


FIG. 4: Radial density distribution function of the He atoms in $\text{Li}^+\text{@He}_{70}$ (solid black line), $\text{Na}^+\text{@He}_{70}$ (dashed line), $\text{Be}^+\text{@He}_{70}$ (red), $\text{Mg}^+\text{@He}_{70}$ (green), $\text{Ca}^+\text{@He}_{70}$ (blue).

two parallel squares, rotated by $\pi/4$ with respect to each other. Indeed, the lowest non-vanishing q_L values for a polyhedron with such a structure correspond to $L = 4$ and $L = 5$. The results reported in Figs. 2 and 3 seem to indicate that $\text{Li}^+\text{@He}_8$ behaves much like a rigid body rather than as an ion embedded within a liquid shell.

B. Multiple-shell ion-doped ^4He clusters

We come now to the main concern of this paper, i.e. to discriminate between solid-like versus liquid-like structures around helium-solvated ions. To this aim we have tried to apply the criterion of Ref. 13 to the more general case of clusters consisting of more than one solvation shell.

Instead of extending the integral in Eq. 4 to the entire cluster, one may calculate multipole moments Q_{LM} of a region within a suitably chosen distance from the center of mass. Thus, the criterion described in the previous Section allows to identify a solid-like behavior of that sub-region of the cluster. In Fig. 4 we show the radial solvent density profiles for 70 ^4He atoms clusters doped with different ions. By taking the first minima of the curves as cut-off distances in the integral which defines Q_{LM} , we accessed the imaginary-time auto-correlation functions of the multipoles of the first shell of the corresponding clusters. Table I reports the integral of the ^4He density within the first solvation shell for the various ions that we have considered.

TABLE I: Integral of the ^4He density distribution within the first solvation shell of $^4\text{He}_{70}$ clusters doped with different ions.

Li^+	Na^+	Be^+	Mg^+	Ca^+
8.24	12.02	14.55	19.02	23.18

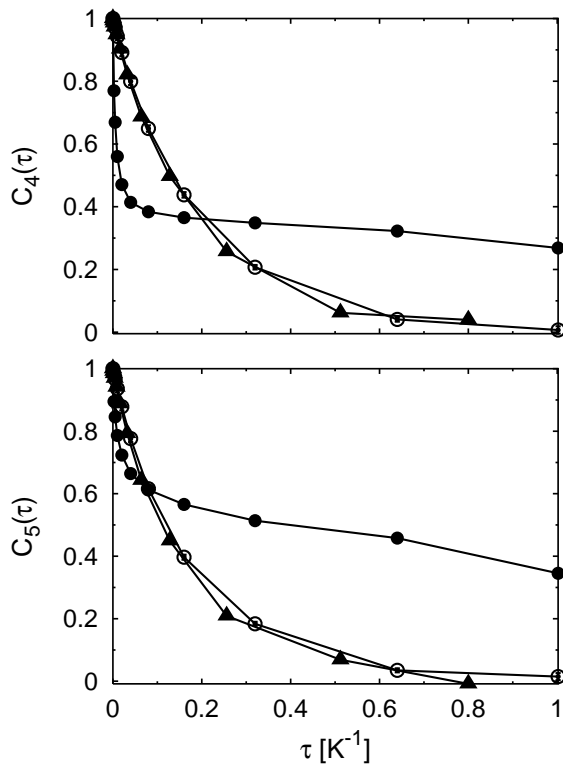


FIG. 5: Comparison of the multipole time-correlation functions $c_L(\tau)$ for $L = 4$ (upper panel) and $L = 5$ (lower panel), as calculated for the whole $\text{Li}^+\text{@He}_{70}$ (empty circles), within the first solvent shell of the same cluster (filled circles), and for CO@He_{15} (triangles).

1. Alkali ions doped ^4He clusters

In Fig. 5 we compare the multipole time-correlation functions $c_L(\tau)$ for $L = 4$ (upper panel) and $L = 5$ (lower panel), as calculated for the first solvation shell in $\text{Li}^+\text{@He}_{70}$, for the same whole cluster, and for CO@He_{15} . The time correlations of the $L = 4$ and $L = 5$ multipoles of the first shell, albeit differing in magnitude, both show a very slow decay (almost a saturation in the case of $L = 4$), whereas the same quantities, when considered for the whole cluster, decay rapidly to zero, very similarly to what happens in CO@He_{15} . Also the $L = 6$ correlation function (not reported) exhibits a slow decay, just slightly more rapid than for the $L = 4$ and $L = 5$ curves. On the contrary, the decay of all the other $c_L(\tau)$ correlations, calculated within the first shell, is extremely fast. We interpret this result as an indication that the ^4He structure in the first solvation shell maintains an average shape, behaving like a solid cage which separates the Li^+ ion from the liquid environment of the outer shells. The signature of the rigidity of the first shell is lost among the random fluctuations in the more external regions, and thus it disappears in the multipole correlations of the entire system.

At least qualitatively, we can attempt a better under-

standing of the behavior of the time-correlations $c_L(\tau)$. In a very simplified and ideal picture, the diffusion of the ^4He atoms of a *solid* first solvation shell during the simulation can be thought as the combination of two kind of motions: one approximately corresponding to a coherent rotation of the whole shell, and the other due to high-frequency small-amplitude fluctuations about the smooth trajectory of the former. When the cluster configurations along the path are rotated backward in order to minimize the particles diffusion, the neat rotation is totally suppressed, whereas the fast fluctuations are not. Thus the only surviving motions can be seen as the incoherent fluctuations of ^4He atoms in the first shell about average positions. More realistically, other motions, not removed by the backward rotation procedure, enter the decomposition of the ^4He atoms diffusion in the first shell. If these motions are sufficiently slow, i.e. if their energies are sufficiently low, the average shape of the first shell is not disrupted too quickly. Correspondingly, since imaginary-time correlation functions can be written as a sum of decaying exponentials whose decaying constants are the excitation energies of the system, the $c_L(\tau)$ correlations, characteristic of the system geometry, exhibit a slow decay.

Within the same qualitative picture, the atoms in the outer regions undergo random motions, none of which is reducible to a neat rotation. The slowest modes of the whole cluster are thus fast enough to prevent the persistence of any global shape (and to produce a rapid decay of the corresponding time-correlations $c_L(\tau)$), but anyway they are much slower than the vibrations of the atoms in the first shell, thus explaining the lower decaying rate of the $c_L(\tau)$ correlation functions at small τ with respect to those of the first shell.

Fig. 6 depicts the ^4He density distribution within the radius of the first shell, where we found an integrated density of ~ 8.24 ^4He atoms. The solvent concentrates mainly in eight regions arranged in two parallel squares rotated by $\pi/4$ with respect to each other. At the opposite poles of this structure, along an axis perpendicular to the planes of the squares, two small lower-density accumulations, probably due to incursions of ^4He density from the second shell, are found (they disappear well before the other eight ones when we increase the isodensity value chosen to draw the picture of Fig. 6). As we explained in discussing $\text{Li}^+\text{@He}_8$, for a two rotated-squares structure the lowest non-vanishing q_L values correspond to $L = 4$ and $L = 5$. We note that the addition of two more vertexes on a line perpendicular to the squares produces a polyhedron having the lowest non-vanishing q_L 's for $L = 5$ and $L = 6$. The behavior of the $c_L(\tau)$ correlation functions can thus be seen as the result of the concomitant signals corresponding to these two structures. We stress at this point the need of considering dynamical correlations $c_L(\tau)$ of the multipoles of the cluster mass density, rather than their static magnitudes q_L , in order to reveal a solid-like behavior of the solvent. In fact, by calculating the quantities q_L of the He density of the first

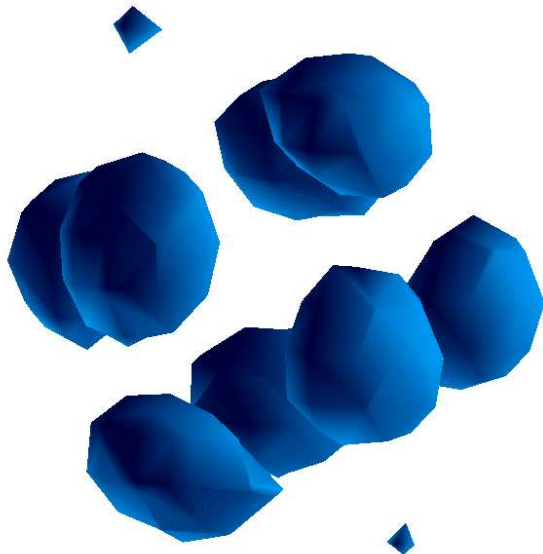


FIG. 6: He density distribution within the first solvation shell of $\text{Li}^+\text{@He}_{70}$. The displayed isosurface contains 60% of the number of He atoms in the first shell. The Li^+ ion is located at the center of the picture, but it is not displayed.

solvation shell of $\text{Li}^+\text{@He}_{70}$, we obtain value at $L = 4$ which is larger but of the same order of magnitude of the value at $L = 3$, whose corresponding imaginary-time correlation function, instead, decays extremely rapidly.

Even more evident is the existence of a solid first shell in clusters doped with a Na cation. Our simulations indicate that the time correlations of the first five multipoles within the first shell decay rapidly, whereas the $L = 6$ shows an extremely slow decay. These results are compatible with an icosahedral structure, whose lowest non-vanishing multipoles correspond to $L = 6$ and $L = 10$. For the first shell of $\text{Na}^+\text{@He}_{70}$, we show in Fig. 7 the slow-decaying $L = 6$ multipole time-correlation function (upper panel) and the ^4He density distribution (lower panel). The latter clearly shows an icosahedral order, in agreement with previous QMC calculations, based on the shadow wave functions technique.¹¹

Interestingly enough, despite the stronger interaction potential characterizing the Li^+ -He pair, we find a more pronounced solid-like behavior of the first shell of ^4He around a Na^+ ion than in the case of Li^+ . This is due to a subtle balance between the depth and the position of the minimum of the He-ion interaction potential, which determines the average number of ^4He atoms in the first solvation shell, and, hence, the average distances among them. For instance, the nearest neighbor He atoms in the first shell of $\text{Li}^+\text{@He}_{70}$ are separated by roughly 2.6 Å, i.e. they find each other in the repulsive region of the He-He interaction potential. In contrast, the nearest neighbor distance in the first shell of $\text{Na}^+\text{@He}_{70}$ is slightly less than 2.8 Å, that is within the well of the He-He pair potential and closer to its minimum (~ 3.0 Å).

The results for $\text{Na}^+\text{@He}_{70}$ have been obtained using

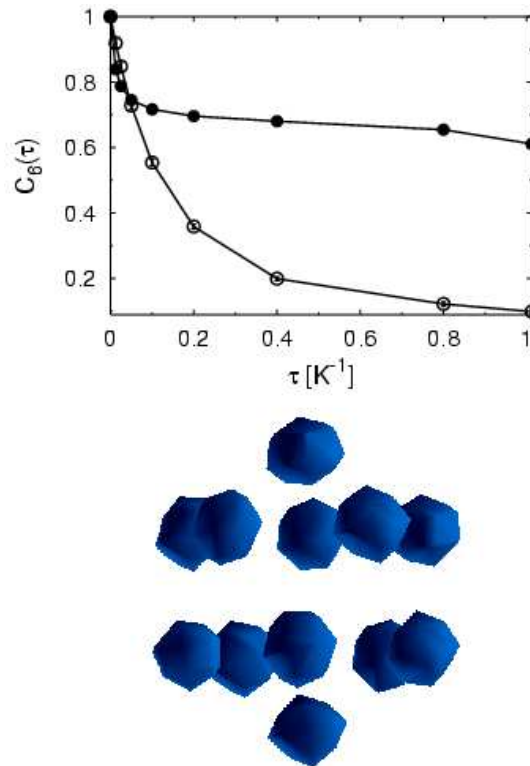


FIG. 7: Upper panel: multipole time-correlation functions $c_L(\tau)$ for $L = 6$, as calculated for the whole $\text{Na}^+\text{@He}_{70}$ cluster (empty circles) and within the first solvent shell (filled circles). Lower panel: He density distribution in the first shell of $\text{Na}^+\text{@He}_{70}$. The isodensity surface contains the 60% of the density of the first shell. The Na^+ ion resides at the center of the structure and it is not displayed.

a time step $\epsilon = 0.0125 \text{ K}^{-1}$. By integrating the ^4He density within the first shell of $\text{Na}^+\text{@He}_{70}$, we obtain an estimate of twelve ^4He atoms, in agreement with shadow wave function and path-integral Monte Carlo (PIMC) results,^{11,27} but at variance with other existing PIMC calculations.¹² Our result is stable, within the statistical error, when reducing the time step by a factor 2.5, thus showing a negligible time-step dependence in this ϵ range. For larger time steps, however, the reliability of the simulations is not guaranteed. In Ref. 12, where a time step of $1/20 \text{ K}^{-1}$ is used, sixteen ^4He atoms are found, instead of twelve, in the first shell of a $\text{Na}^+\text{@He}_{100}$ cluster at the temperature of 1 K. The above discrepancy may originate from the choice of the He- Na^+ interaction potential¹² or, more likely, it is a time-step effect. In fact, for strongly attractive potentials, such as the Li^+ -He and the Na^+ -He ones, we noted that the use of a large time step (like the one used in Ref.12) may lead to overestimate the ^4He density in the first shell. In particular, by simulating $\text{Na}^+\text{@He}_{70}$ with the same rather large time step $\epsilon = 0.05 \text{ K}^{-1}$, we reproduced the result of Ref. 12. We also observed that the ^4He density in the first solvation shell is much more delocalized, lacking

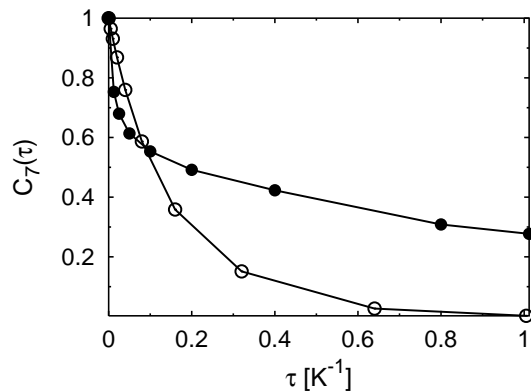


FIG. 8: Multipole time-correlation functions $c_L(\tau)$ for $L = 7$, as calculated for the whole $\text{Be}^+\text{@He}_{70}$ cluster (empty circles) and within the first solvation shell (filled circles).

the icosahedral structure previously found, and that the lowest twelve multipoles time-correlation functions decay now much more rapidly.

2. Alkaline-earth ions doped ^4He clusters

We now turn our attention to the case of ^4He clusters doped with alkaline-earth ions. Due to their larger radii and their relatively weaker interactions with helium atoms, these ions are expected to give rise to bubble-like structures of the ^4He liquid around the impurity. This expectation is confirmed by mobility measurements at finite temperature for several alkaline-earth ions but not for Be^+ , for which results of similar measurements suggest instead a snowball structure of the defect.⁶ For this reason, in the following, we will focus particularly on the solvent structure around Be^+ . The rigidity of the defect structures of Be^+ and Mg^+ can hardly be distinguished on the basis of static correlation functions among ^4He atoms,¹⁴ thus spurring us to consider the multipole moments dynamical correlations criterion.¹³

In order to detect even weak signatures of a possible solid-like order around the alkaline-earth ions, the clusters configurations, used for calculating both static and dynamical quantities, have been rotated back in order to minimize the particles diffusion within the *first* solvation shell, and not in the whole clusters. According to our results, all the multipoles correlations of the first shell of $\text{Be}^+\text{@He}_{70}$ up to $L = 5$ decay rapidly (even faster than in the whole cluster), whereas for $L = 6$ and, more evidently, for $L = 7$ the correlation decay is much slower than that of the whole cluster. Also in this case the magnitude of the multipoles q_L provide a guide in the search of the slow decaying time-correlations. Fig. 8 displays the $L = 7$ multipole correlation in the first solvation shell and in the whole cluster. In spite of the faster decay than for $\text{Li}^+\text{@He}_{70}$ and $\text{Na}^+\text{@He}_{70}$, the behavior of $c_L(\tau)$, for $L = 7$, indicates an extremely slow disappearance of the

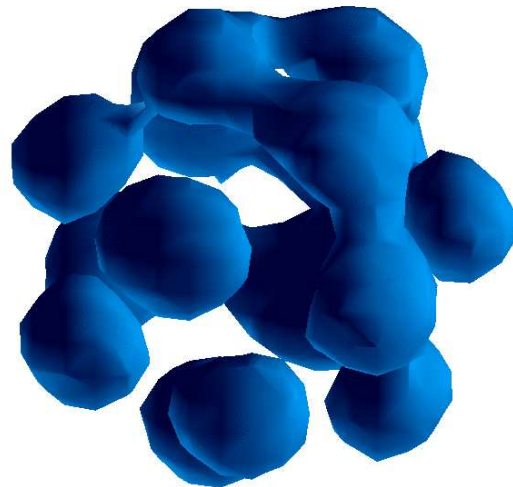


FIG. 9: He density distribution in the first shell of $\text{Be}^+\text{@He}_{70}$. The isodensity surface contains the 60% of the density of the first shell. The Be^+ ion resides at the center of the structure and it is not displayed.

shape assumed by the solvent around the Be^+ ion. The average shape of the solvent in the first shell is shown in Fig. 9. Despite being less localized than for alkali ion doped clusters, the ^4He density in the vicinity of Be^+ appears anyway significantly structured.

Fig. 10 compares the diffusion coefficient in imaginary time, $D(\tau)$, as calculated after the backward rotation, for the ^4He atom in the whole cluster and within the first shell, for $\text{Li}^+\text{@He}_{70}$ and $\text{Be}^+\text{@He}_{70}$. For both systems, with increasing the (imaginary) time τ , the coefficient $D(\tau)$ of the whole cluster increases much more than within the first solvation shell, due to the liquid character of the external regions. We interpret the small diffusion rate of the He atoms in the first shell, and, moreover, the close similarities in $D(\tau)$ for $\text{Be}^+\text{@He}_{70}$ and $\text{Li}^+\text{@He}_{70}$ (which we consider a prototype of a cluster with a first shell with solid-like order) as an indication of a nearly rigid-body behavior of the first shell of $\text{Be}^+\text{@He}_{70}$. This conclusion will be strengthened by the comparison with the results for $\text{Mg}^+\text{@He}_{70}$, which will be discussed next.

For $\text{Mg}^+\text{@He}_{70}$ the calculation of q_L , within the first solvation shell, gives a faint signal for $L = 8$. However, the corresponding imaginary-time correlation function $c_L(\tau)$, which is reported in Fig. 11, exhibits an extremely fast decay, despite being the slowest decaying one among those we have analyzed (up to $L = 12$). Our findings suggest that the He atoms surrounding Mg^+ undergo random fluctuations which disrupt the local structure of the solvent much more quickly than in the other cases examined so far, thus preventing the formation of any longly persisting solid-like order. For $\text{Mg}^+\text{@He}_{70}$ the rapid decaying of the $c_L(\tau)$ correlations of the first shell is very similar to that of the corresponding ones of the entire cluster, thus indicating a liquid-like behavior of the

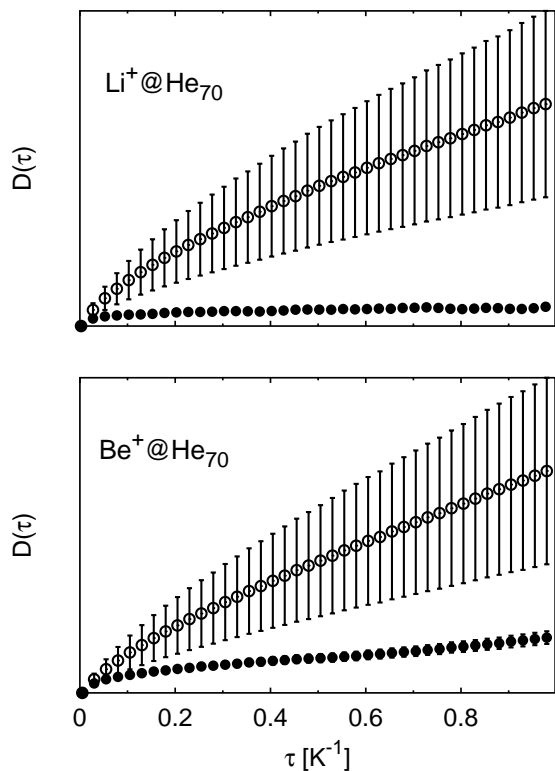


FIG. 10: Upper panel: diffusion coefficient $D(\tau)$ as a function of (imaginary) time τ calculated from the backward-rotated configurations, for the He atoms in the whole $\text{Li}^+\text{@He}_{70}$ cluster (empty circles), and for the He atoms in its first solvation shell (filled circles). Lower panel: same quantities for $\text{Be}^+\text{@He}_{70}$, displayed with the same symbols.

whole system.

As it is shown in the upper panel of Fig. 12, the ^4He density distribution in the first shell is considerably more diffuse than what found for the other ions. By increasing the isodensity value chosen for the graph, it becomes possible to identify regions of higher density, nevertheless the solvent is much more delocalized than for $\text{Be}^+\text{@He}_{70}$.

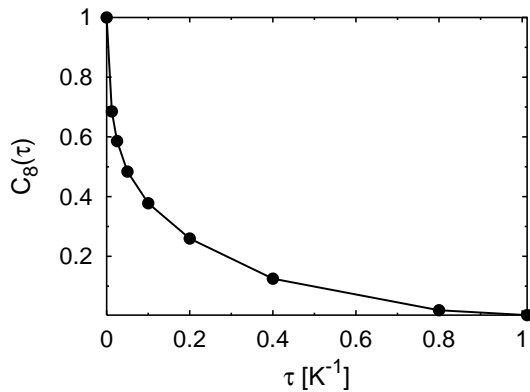


FIG. 11: Multipole time-correlation function $c_L(\tau)$ for $L = 8$, as calculated within the first solvation shell of $\text{Mg}^+\text{@He}_{70}$.

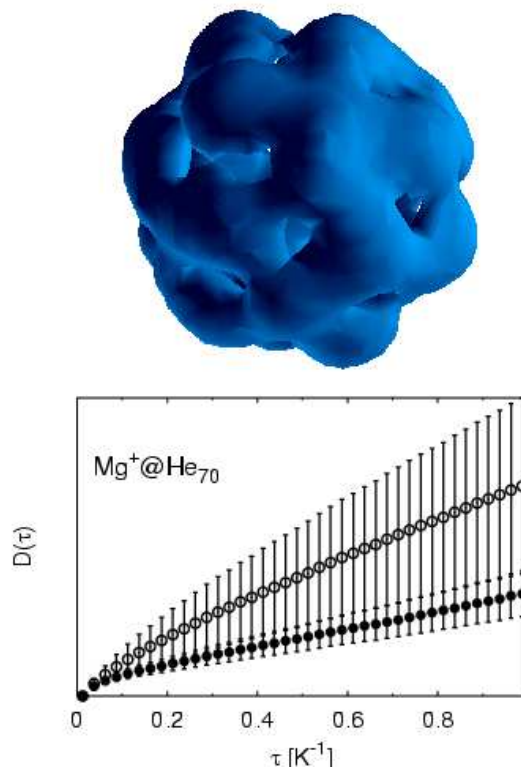


FIG. 12: Upper panel: He density distribution in the first shell of $\text{Mg}^+\text{@He}_{70}$. The integral of the density contained within the displayed isodensity surface amounts to 60% of the number of He atoms in the first shell. Lower panel: diffusion coefficient $D(\tau)$ as a function of (imaginary) time τ for the He atoms in $\text{Mg}^+\text{@He}_{70}$, as calculated from the backward-rotated configurations, for the whole cluster (empty circles) and for the first solvation shell (filled circles).

The lower panel of Fig. 12 compares the imaginary-time diffusion of the ^4He atoms in the entire cluster and in the first solvation shell, after the backward rotation. The two curves are now closer and they even merge within the error bars, thus proving that the rotational diffusion of the particles in the first shell cannot be reduced to a neat rotation. The liquid-like behavior of the solvent is even more evident in $\text{Ca}^+\text{@He}_{70}$, for which the first shell multipole time-correlation functions decay very rapidly, the density distribution in the first solvation shell is largely delocalized and the diffusion coefficients of ^4He atoms of the inner and of the outer shells are much less distinguishable.

IV. CONCLUSIONS

Using PIGS simulations, we have studied the solvation of alkali and alkaline-earth ions in ^4He clusters. In order to discriminate between solid-like versus liquid-like behavior of the solvent in the vicinity of the impurity, we employed a criterion based on dynamical correlations

of the multipole moments of the ^4He density in the first shell, previously proposed for quantum clusters consisting of just one completed shell. We also used other indicators to clarify the structure of ^4He around the impurity.

The dynamical correlations criterion, whose applicability to clusters with more than one shell was not granted a priori, proved suitable to address situations in which regions with different rigidity coexist within the system, without requiring any prior knowledge of the defect structure. In particular we find bubble (liquid-like) structures for heavier alkaline-earth ions (Mg^+ and Ca^+), whereas alkali-ions are caged by a solid-like, snowball structure, further embedded in an outer liquid environment. For

these two categories, whose features are expected to be different both theoretically^{3,4} and experimentally,^{5,6} the multipole correlations signatures are clearly different and unambiguously distinguishable.

For Be^+ , our simulations indicate a border-line behavior, which, however, has much more similarities with alkali ions than with heavier alkaline-earth ones. This results suggests that Be^+ forms a snowball upon solvation, possibly elucidating the “anomalous” mobility of Be^+ in liquid helium with respect to Mg^+ , Ca^+ and other alkaline-earth ions.⁶

-
- * Electronic address: stefano.paolini@pd.infn.it
 † Electronic address: francesco.ancilotto@pd.infn.it
 ‡ Electronic address: flavio.toigo@pd.infn.it
- ¹ A. L. Fetter, in *The Physics of Liquid Helium*, edited by K. H. Bennemann and J. B. Ketterson (Wiley, New York, 1976).
 - ² K. R. Atkins, *Phys. Rev.* **116**, 1339 (1959).
 - ³ M. W. Cole and R. A. Bachman, *Phys. Rev. B* **15**, 1388 (1977).
 - ⁴ M. W. Cole and F. Toigo, *Phys. Rev. B* **17**, 2054 (1978).
 - ⁵ W. I. Glaberson and W. W. Johnson, *J. Low Temp. Phys.* **20**, 313 (1975).
 - ⁶ M. Foerste, H. Guenther, O. Riediger, J. Wiebe, and G. zu Pultitz, *Z. Phys. B: Condens. Matter* **104**, 317 (1997).
 - ⁷ P. Claas, S. -O. Mende, and F. Stienkemeier, *Rev. Sci. Instrum.* **74**, 4071 (2003).
 - ⁸ J. P. Toennies and A. F. Vilesov, *Angew. Chem. Int. Ed.* **43**, 2622 (2004).
 - ⁹ F. Stienkemeier and K. K. Lehmann, *J. Phys. B* **39**, R127 (2006)
 - ¹⁰ M. Barranco, R. Guardiola, S. Hernández, R. Mayol, and M. Pi. *J. Low Temp. Phys.* **142**, 1 (2006).
 - ¹¹ M. Buzzacchi, D. E. Galli, and L. Reatto, *Phys. Rev. B* **64**, 094512 (2001).
 - ¹² A. Nakayama and K. Yamashita, *J. Chem. Phys.* **112**, 10966 (2000).
 - ¹³ S. Baroni and S. Moroni, *ChemPhysChem* **6**, 1884 (2005).
 - ¹⁴ M. Rossi, M. Verona, D. E. Galli, and L. Reatto, *Phys. Rev. B* **69**, 212510 (2004).
 - ¹⁵ K. K. Lehmann, *Phys. Rev. Lett.* **88**, 145301 (2002).
 - ¹⁶ S. Baroni and S. Moroni, in *Quantum Monte Carlo Methods in Physics and Chemistry*, edited by P. Nightingale and C.J. Umrigar. NATO ASI Series, Series C, Mathematical and Physical Sciences, Vol. 525, (Kluwer Academic Publishers, Boston, 1999), p. 313, also available at [cond-mat/9808213](#).
 - ¹⁷ S. Baroni and S. Moroni, *Phys. Rev. Lett.* **82**, 4745 (1999).
 - ¹⁸ A. Sarsa, K. E. Schmidt, W. R. Magro, *J. Chem. Phys.* **113**, 1366 (2000).
 - ¹⁹ M. T. Elford, I. Røeggen, and H. R. Skullerud, *J. Phys. B* **32**, 1873 (1999).
 - ²⁰ E. Czuchaj, F. Rebentrost, H. Stoll, H. Preuss, *Chem. Phys.* **207**, 51 (1996).
 - ²¹ The He-He interactions are calculated by the potentials given in A. Aziz, A. R. Janzen, M. R. Moldover, *Phys. Rev. Letts.* **74**, 1586 (1995) for ion-doped clusters and in T. Korona, H. L. Williams, R. Bukowski, B. Jeziorski and K. Szalewicz, *J. Chem. Phys.* **106**, 5109 (1997) for the CO-doped one.
 - ²² T. G. A. Heijmen, R. Moszynski, P. E. S. Wormer, and A. van der Avoird, *J. Chem. Phys.* **107**, 9921 (1997).
 - ²³ R. Alrichs, H. J. Bohm, S. Brode, K. T. Tang, and J. P. Toennies, *J. Chem. Phys.* **88**, 6290 (1988).
 - ²⁴ D. Bellert and W. H. Beckenridge, *Chem. Rev. (Washington, D. C.)* **102**, 1595 (2002).
 - ²⁵ P. Cazzato, S. Paolini, S. Moroni, and S. Baroni, *J. Chem. Phys.* **120**, 9071 (2004)
 - ²⁶ D. M. Ceperley, *Rev. Mod. Phys.* **67**, 279 (1995).
 - ²⁷ M. Rossi, PhD. Thesis (2006)